Cloud bands in the earth's atmosphere

Observations and Theory

By JOACHIM P. KUETTNER, *National Oceanic and Atmospheric Administration Boulder, Colorado, USA*

(Manuscript reveived January 15, 1971; revided version June 22, 1971)

ABSTRACT

It is now well known that parallel cloud bands are widespread in the earth's atmosphere. Observations from manned and unmanned spacecraft and from high-altitude aircraft in connection with soundings from ships and ground stations have shed light on their origin. These and a special investigation of tropical cloudstreets during the BOMEX Project suggest the following typical characteristics of convective cloudstreets: Length = 20 to 500 km; spacing = 2 to 8 km; layer height = 0.8 to 2 km; width-to-height ratio = 2 to 4; wind structure: little change of direction with height; vertical gradient of wind shear (profile curvature) = 10^{-7} to 10^{-6} cm^{-1} sec^{-1}; alignment: along the mean wind of the convective layer.

On the theoretical side, linear wind shear is known to favor convective "streeting". The present theory investigates the effect of the observed profile curvature neglecting linear shear effects. It shows that the curvature itself enforces alignment of convective cells with the flow direction. Inertial forces arising from the vorticity field counteract buoyancy forces. Their ratio as expressed in a modified Froude numer determines the value of the critical Rayleigh number responsible for the onset of convection. In a flowing medium this number is raised, often by several orders of magnitude, over that of a resting medium for all convective modes, except the longitudinal mode. Some three-dimensional computer presentations illustrate these results.

A quantitative application of the simplified theory to actual atmospheric conditions is attempted. It indicates that in strong flows heated from below longitudinal rolls may double their amplitude in a matter of 10 minutes while transverse rolls decay at a similar rate with symmetric cells having nearly neutral stability.

The relations of this concept to other hypotheses and to the Goertler/Taylor rolls are discussed. Finally it is speculated that the formation of wind streaks on water surfaces may be related to a similar mechanism.

Introduction

The banded cloud structure of the earth's atmosphere, hardly noticeable from the ground, revealed itself to the meteorological observer when aviation offered the opportunity to view clouds from sufficient heights. Birds and human soaring pilots utilizing the banded updrafts in the subcloud layer identified them as convective phenomena connected with strong winds (Woodcook, 1942; Kuettner, 1947, 1959).Since the event of spaceflight, weather satellites and photographs from manned spacecraft have established cloud streets of different scales as a common characteristic of the atmosphere. In an earlier investigation, conducted just prior to the first earth oriented satellites (Kuettner, 1959; to be called "Part I" from here on), the band structure of the atmosphere was found to originate in convective layers with higher than normal winds and a curved vertical velocity profile of rather uniform direction. These findings were attributed to the thermal wind conditions connected with large scale "heated flows" in the boundary layer advecting cold air over warm surfaces.

In a preliminary theoretical note on the underlying mechanism contained in Part I, it was pointed out that longitudinal rolls are the preferred convective mode of a flow in which buoyancy forces are counteracted by vorticity forces arising from the vertical shear gradient.

It was also stated that "in Part II to be published separately, the theory of this type of organized convection will be discussed." The present article constitutes a much delayed fulfillment of this pledge.

In the meantime considerable work of observational and theoretical nature has been published. Schuetz & Fritz (1961) have investigated cloud streets over the Caribbean Sea as seen by a narrow angle television camera from TIROS I. The findings of Part I were generally confirmed. The thorough analysis of three long-distance flights over the Pacific Ocean (Malkus & Riehl, 1964*a* and *b*) contains a wealth of information on organized convection over the tropical oceans. Of specific interest is the description of the superimposed "parallel" and "crosswind" modes which the authors attribute to shearing layers at different heights. (This study also shows what it takes to analyse atmospheric cloud patterns from aircraft flying at moderate heights.) In another study, Plank (1966) investigated cumulus patterns over Florida during a summer month and analysed them with respect to the wind conditions. His results did not corroborate the findings of Part I and were considered inconclusive. Konrad (1968) has investigated the alignment of convective cells in clear air by powerful radars concluding that "clear air thermal streeting" is connected with a vertical wind structure essentially unidirectional with the thermal streets. Further, he found a decided curvature in the wind profile whose magnitude agrees with the findings of Part I, but "may be much higher locally, i.e., by an order of magnitude". Spacing between streets was roughly twice the height of the convective layer. Konrad's results indicate that condensation is not essential to the formation of convective streets, in agreement with the experience of glider pilots who have used "dry streets" in straight flight.

The enormous amount of pictorial information by the long, successful series of weather satellites has produced many practical applications. Today cloud bands are used operationally as approximate indicators of the flow direction by experienced personnel concerned with daily synoptic nephanalysis (Anderson, Ferguson & Oliver, 1966; Anderson et al., 1969).

Many cloud streets, specifically over the subtropical and tropical oceans, islands and coastal areas are however beyond the resolving power of present synoptic satellite cameras. In these latitudes color photographs taken by the Mercury, Gemini and Apollo astronauts give impressive testimony to the abundance of cloud bands. Samples of these pictures are given in Kuettner & Soules (1966). Gaby (1967) using satellite and conventional data has investigated cloudstreets over the tropical oceans and their relation to the surface winds and has found that a very large majority of cumulus lines in equatorial latitudes is oriented parallel to the surface winds.

Also, the interesting balloon measurements of helical circulations in the boundary layer by Gifford (1953) and by Angell, Pack & Dickson (1968) should be mentioned here. They represent counterrotating (helical) longitudinal roll vortices of about 4 km separation. Hanna (1969) presents evidence that the widespread occurrence of longitudinal sand dunes often seen on astronaut photographs is due to convective circulations oriented along the direction of the prevailing winds.

Theoretical work has likewise advanced rapidly in the last few years. Faller (1963), in experiments with rotating fluids which have a radial flow component towards the center, found spiral bands resembling those in hurricanes. The bands are oriented at an angle to the left of the free geostrophic flow on top of the boundary layer, i.e., they approximate the direction of flow at some intermediate level within the boundary layer. Extending these findings he has proposed to apply them to the formation of normal atmospheric cloud streets (Faller, 1965). Barcilon (1965) studying two-dimensional waves in a non-divergent Ekman layer (without radial flow) finds equivalence of the Ekman instability to that of a classical boundary layer in parallel flow whose vertical profile is given by the projection of the Ekman velocity components on a vertical plane. Faller & Kaylor (1966) studied numerically the instability of a laminar Ekman boundary layer. Lilly (1966) has shown that two types of instability are involved in Faller's experiments, one being inviscid and connected with an inflection point in the component normal to the basic flow, the other being a new mechanism of instability dependent on the Coriolis effect. Brown (1970) has shown that finite two-dimensional perturbations (helical rolls) in a neutrally buoyant fluid tend to alter the dynamically unstable Ekman

flow profile so that it becomes stable in combination with the secondary flow. These studies on the stability of the Ekman layer in the absence of buoyancy forces are of general interest to atmospheric flows with directional shear, although the case of precisely neutral stability is probably rare in the atmosphere.

Also the unstable modes of parallel flow with linear shear (Couette flow) have been studied in connection with atmospheric convection bands. Kuo (1963) found that for small negative values of the Richardson number longitudinal bands will be the dominant form of convection while for large negative values transverse waves will also be excited. Kuo attributes these findings to the (stabilizing) effect of the Couette flow on disturbances oriented across the flow. While Kuo assumed a Prandtl number of unity, the work of Deardorff (1965) and of Gallagher & Mercer (1965) deals with Couette flow at different Prandtl numbers. Only two-dimensional disturbances were considered. The stabilizing effect of shear on disturbances oriented across the flow is expressed by the critical Rayleigh number as a function of Reynolds number and Prandtl number. High Reynolds and Prandtl numbers raise the critical Rayleigh number for these disturbances, favoring the longitudinal mode. The physical process by which Couette flow stabilizes transverse perturbations has been elucidated by Asai (1970), who has shown that, through upwards transport of momentum, kinetic energy of the perturbation is transformed into that of the basic flow, draining the reservoir of potential energy contained in the unstably stratified fluid. This however, is not true for longitudinal disturbances.

As pointed out earlier, the vertical wind profiles in the atmospheric boundary layer found under conditions of cloudstreet development rarely resemble pure Couette flow and are frequently curved. Also the veering of wind with height as postulated by Ekman flow is not typical; little directional change with height is common and even backing rather than veering is found as a consequence of the baroclinic situation.

While the vorticity in Couette flow is constant with height, it has a vertical gradient in curved velocity profiles. Therefore, the conservation and the vertical transport of differential vorticity by convective motions become important factors and the mechanism is quite

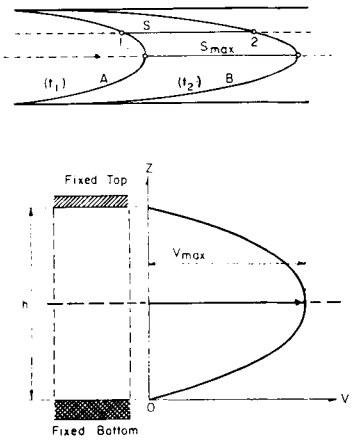

Fig. 1. Laboratory experiments producing longitudinal convection bands. (Avsec, 1939). Bottom: Velocity profile of air moving between fixed top and bottom boundaries. Top: Displacement s between times t_1 and t_2.

different from that responsible for bands in Couette flow. A preliminary treatment of this problem was given by Kuettner (1967). Gage & Reid (1968) have studied the general stability problem in stratified plane Poisseuille flow. Chapter II of this paper will say more about the theory of organized convection in atmospheric boundary layer flows with curved wind profiles.

Finally, the laboratory experiments on cellular convection in resting and flowing media must be mentioned here. Following Bénard's (1900, 1927) classical work most of these experiments were conducted prior to World War II, culminating in Avsec's (1939) magnificent monograph. The development of longitudinal rolls was observed in flowing media heated from below, when (1) the top and bottom boundaries were fixed—resulting in a curved velocity profile (Terada, 1928; Avsec, 1939), see also Fig. 1 and 2—or (2) when the top boundary moved relative to the bottom boundary—resulting in a Couette-like flow (Graham, 1933; Chandra, 1938). The similarity of these laboratory experiments to atmospheric cloud formations has often been noted, for example by Mal (1931), and Brunt (1951).

I. Observations in the Atmosphere

The pictorial and aerological material of Part I was based primarily on ground and airborne

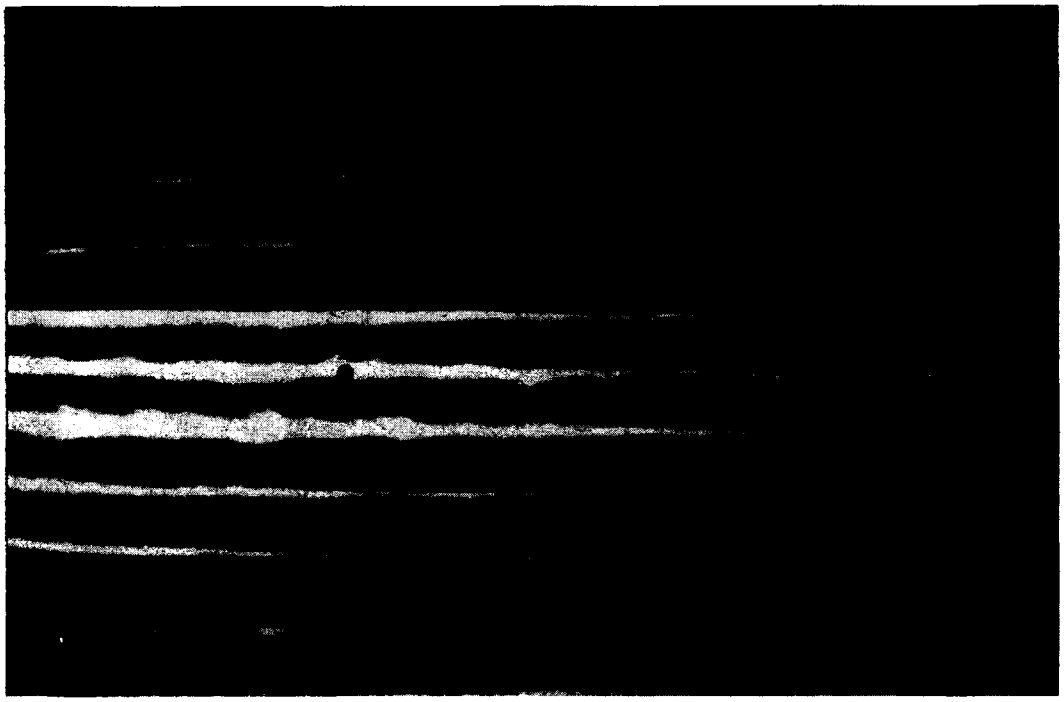

Fig. 2. Longitudinal convection bands in air heated from below (Avsec, 1939) using tobacco smoke.

observations. Since then, cloud photography from very high flying aircraft (U-2, RB-57F, etc.) and from spacecraft has revealed the full extension of the banded structure of the atmosphere on many scales. The following material refers primarily to the convective scale and the planetary boundary layer.

Detailed results of a special study on cloudstreets during the BOMEX Project conducted over the tropical Atlantic in 1969 (Kuettner & Holland, 1969) are being published separately. Here only two examples will be given: Fig. 3 shows typical cumulus streets in the trade wind layer as observed from the NASA Convair 990 (Photo Dr Marlatt) on July 25, 1969 during this project, and Fig. 4 gives a panoramic view of cloudstreets over the BOMEX area photographed from a RB-57F at about 52 000 ft on June 28, 1969. (The "global" appearance is a wide-angle-lens effect.) The orientation of the bands in Fig. 4 is roughly from 100° to 280° and their average spacing about 3 km. Fig. 5 shows the corresponding radar wind sounding from the oceanographic ship "Discoverer" stationed close to the photographed area. Average wind direction in the trade-wind layer and orientation of the cloudstreets coincide, as usual, within about 10° and the wind profile shows a characteristic curvature of about 2×10^{-7} cm^{-1} sec^{-1}. If the layer depth is about 1.5 km, the width/height ratio of the bands is near 2. During the BOMEX Project cloudstreets were observed directly over the equator (Coriolis acceleration $f = 0$). A total of 69 observations from the ship "Mt Mitchell" on the orientation of cloudstreets with respect to surface winds and wavecrests indicate that their alignment is very close indeed to the prevailing wind direction (Fig. 6).

As has been mentioned earlier, excellent information is now available from unmanned and manned spacecraft. Fig. 7 gives a view of the cloud cover over Florida from the Mercury Redstone spacecraft MR-2 shortly after liftoff on Jan. 31, 1961, with a virtually simultaneous aerological sounding from Cape Kennedy (Fig. 8). The cloudstreets are oriented in the general wind direction and the wind profile is curved with about 2×10^{-7} cm^{-1}/sec^{-1}. The layer depth is roughly 1.2 km.

Fig. 3. Cloudstreets over the tropical Atlantic as seen from NASA Convair 990 at 30 000 feet on July 25, 1970 during Bomex Project. (Photo Marlatt.)

Some examples from meteorological satellites follow. Fig. 9 is a "Nimbus" picture of Wisconsin showing cloudstreets up to 150 km in length, spaced about 5 km apart on August 30, 1964. The pibal of Greenbay (Fig. 10) suggests a layer depth of 1.2 km and a curvature of about 4.5×10^{-7} cm^{-1} sec^{-1}. Orientation and wind direction in the convective layer roughly coincide and the width/height ratio is near 4. Fig. 11 shows the outflow of arctic air ($-10°$ to $-30°$C) over the open Gulf of St. Lawrence on Feb. 4, 1963. The developing vigorous convection over the warm water is organized in snow bands, reaching over 500 km length and spaced approximately 8 km apart. (There are probably further subdivisions but these cannot be resolved with the vidicon camera of this spacecraft.) The early morning soundings west and east of the Gulf (Fig. 12) suggest strong west-north-westerly winds with a curvature of 2 to 3×10^{-7} cm^{-1} sec^{-1}. There is little change of wind direction with height and slight backing may be noted.

The most impressive high resolution views of global cloud cover have come from manned spacecraft in low orbits. Some of these were published in an earlier paper (Kuettner & Soules, 1967). In Fig. 13, we show the exquisite Apollo 6 picture of widespread convective bands developing in a southerly flow inland of the coastline of Georgia on April 4, 1968. Many of these bands extend over 100 km in length. Their average spacing is between 2 and 2.5 km. The morning sounding of Jacksonville, Florida, which is just south of the lower right corner of the picture shows a layer depth of about 0.8 km with strong curvature (7×10^{-7} cm^{-1} sec^{-1}) (Fig. 14); the shear near the ground is likewise high (3×10^{-2} sec^{-1}). The width/height ratio seems to lie between 2.5 and 3.

In general these observations resemble the preliminary findings of Part I, the numerical values of the vorticity gradient being somewhat higher than originally expected. Directional changes of the wind in the convective layer are small. Our conclusions may be summarized by stating that convective cloudbands in the earth's atmosphere tend to form in strong flows heated from below with a curved velocity profile

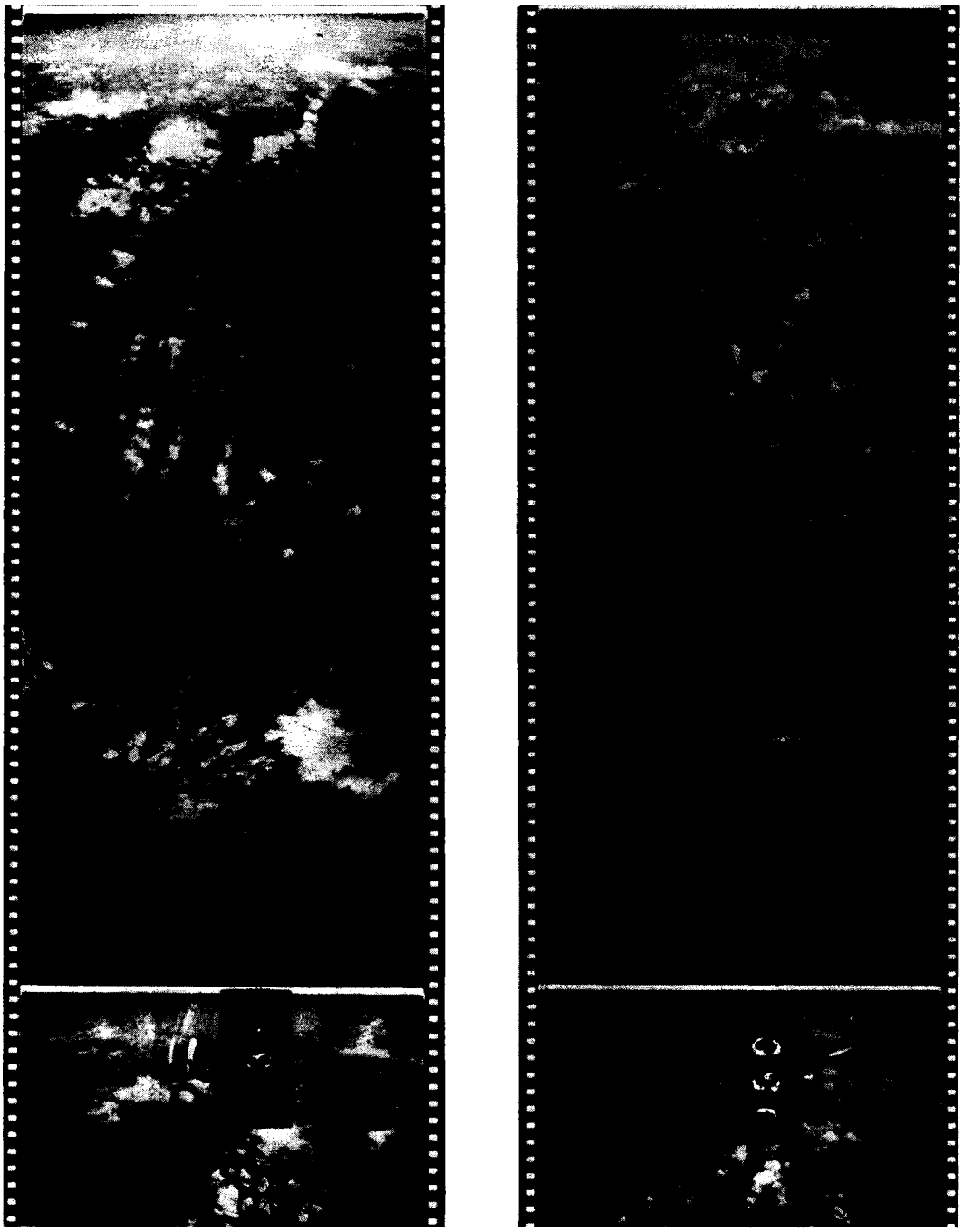

Fig. 4. Wide-angle view of cloudbands over Bomex array as seen from USAF RB-57F at 52 000 ft on June 28, 1970. Cloudstreets are oriented from approximately 100° to 280°. Average spacing: 3 km. Aircraft flying from left to right on each frame.

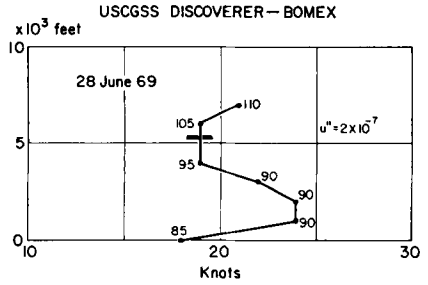

Fig. 5. Rawinsonde from ship "Discoverer" near location and time of high altitude photos, Fig. 4. Numbers along curve are wind directions in degrees. Average curvature, $\overline{u''}$ (in cm^{-1}/sec^{-1}) of velocity profile is also noted. Solid bar marks estimated top of convective layer.

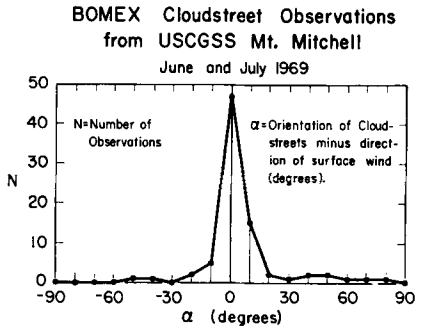

Fig. 6. Orientation of tropical cloud bands with respect to surface winds as observed by the oceanographic ship "Mt. Mitchell" during BOMEX Project (69 cases).

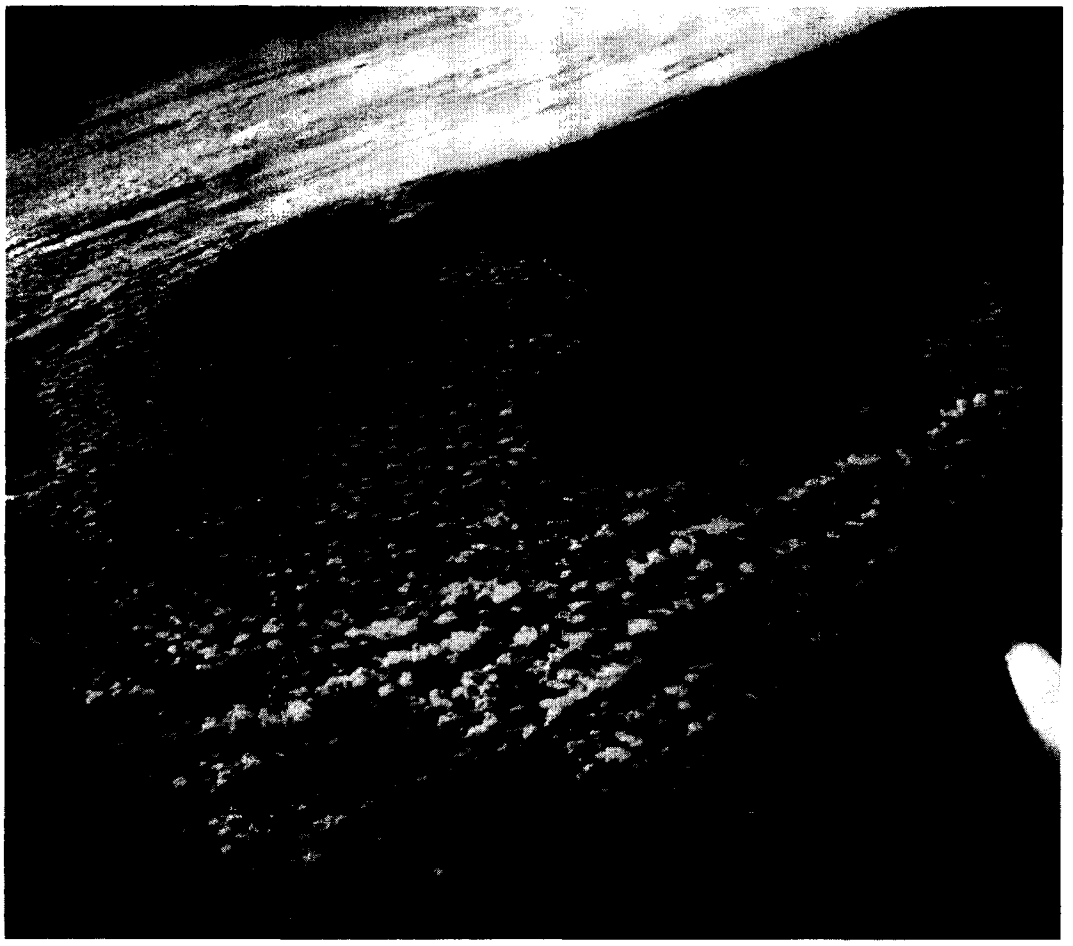

Fig. 7. View of cloustreets over Florida r ear Cape Kennedy as taken from Mercury Redstone spacecraft Mr-2 on January 31, 1961. (Photo NASA.)

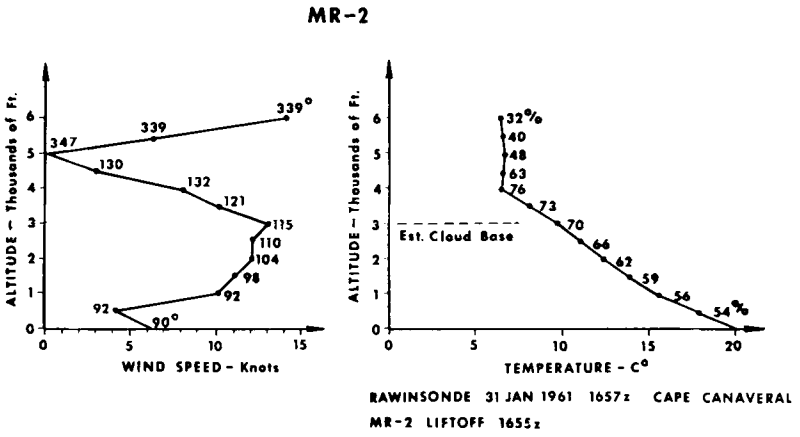

Fig. 8. Special rawin sounding taken during MR-2 launch at Cape Kennedy on January 31, 1961 (Fig. 7). Numbers on left curve are wind directions, numbers on right curve are relative humidities.

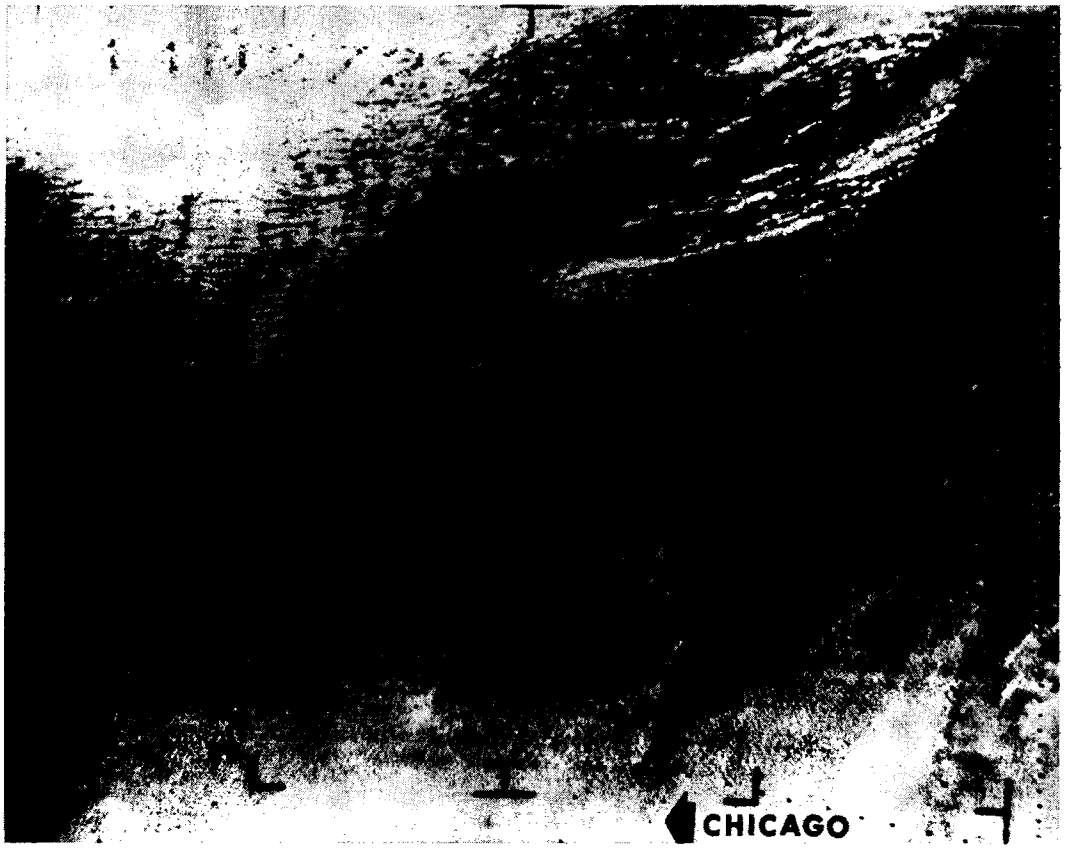

Fig. 9. "Nimbus" satellite picture of cloudstreets over Wisconsin taken on August 30, 1964. Maximum length of band: 150 km, average spacing: 5 km.

of rather uniform direction. Typical values found are as follows: Length of cloudstreets: 20 to 500 km; spacing: 2 to 8 km; layer height: 0.8 to 2 km; width/height ratio: 2 to 4; vertical shear gradient: 10^{-7} to 10^{-6} cm^{-1} sec^{-1}

II. Theory

It may help to briefly describe the physical mechanism underlying the subsequent theoretical derivation.

1. Brief Description of Physical Mechanism

Our observational findings suggest that vorticity forces (forces associated with profile curvature) enter the convective mechanism. In using the term "vorticity", it should be understood that we are talking about vorticity around a horizontal axis normal to the basic flow direction, i.e. the y component of vorticity. Assuming parallel flow in the x direction, this vorticity is essentially given by the vertical shear of the horizontal wind. It is known that the restoring forces experienced by a displaced parcel conserving its vorticity in an environment of varying vorticity tend to return the parcel to its original level. This mechanism also underlies the Rossby waves in the westerlies and the Tollmien–Schlichting waves in the boundary layer. It may be visualized as follows (Lin, 1955):

In a normal boundary layer the velocity profile is curved and the vorticity is decreasing upwards, i.e., a horizontal layer near the ground has a higher vorticity (shear) than an layer near the top (Fig. 15, left); the vorticity gradient is negative ($\partial^2 u/\partial z^2 < 0$). If a fluid element from a lower level is displaced upwards it conserves its vorticity and constitues a "relative vortex" having an excess vorticity over its new environment. (Fig. 15, right.) The resulting distortion of the basic vorticity field causes fluid elements on the left side of the vortex to be replaced by elements from lower levels (having an excess vorticity) and those on the right side by elements from higher levels (having a vorticity deficiency). This redistribution induces a downward acceleration of the "vortex" returning the displaced element toward the level where it belonged and where it finds no differential vorticity.

This mechanism applies to every vertically displaced element, as long as the vorticity

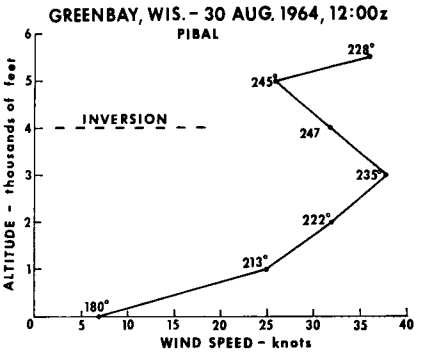

Fig. 10. Pibal sounding taken at Green Bay, Wisconsin on August 30, 1964, 12: 00 Z. (Fig. 9.) Numers along curve are wind directions.

gradient does not change sign. The motion is therefore stable (If the vorticity gradient changes sign, i.e., if there is an inflection point in the velocity profile an element displaced through this inflection point may "find a home" of equal vorticity on the other side of the inflection point, resulting in the well-known inviscid instability.)

Fluid elements displaced upwards or downwards under the action of buoyancy forces will therefore have to overcome the restoring forces resulting from the vorticity gradient. Nature can circumvent this restriction of convective motion by selecting a specific mode of convection in which such restoring forces cannot arise: If all fluid elements along a horizontal line in the direction of flow organize themselves to move upwards simultaneously and complete their circulation in a plane normal to the x, z plane, no differential vorticities can develop between them in the x, z plane and convection is uninhibited by restoring forces. This mode of organized convection represents helical motions in longitudinal rolls, the precise dimensions of which are regulated by other factors such as viscosity. It should be noted that in the y, z plane the convective circulations do not encounter restoring forces either because in this plane there exists no basic flow and therefore no vorticity gradient.

One can derive this mechanism more rigorously by introducing the vorticity gradient into the equations of the classical theory of cellular convection (Rayleigh, 1916). The results of this theory are then modified as follows:

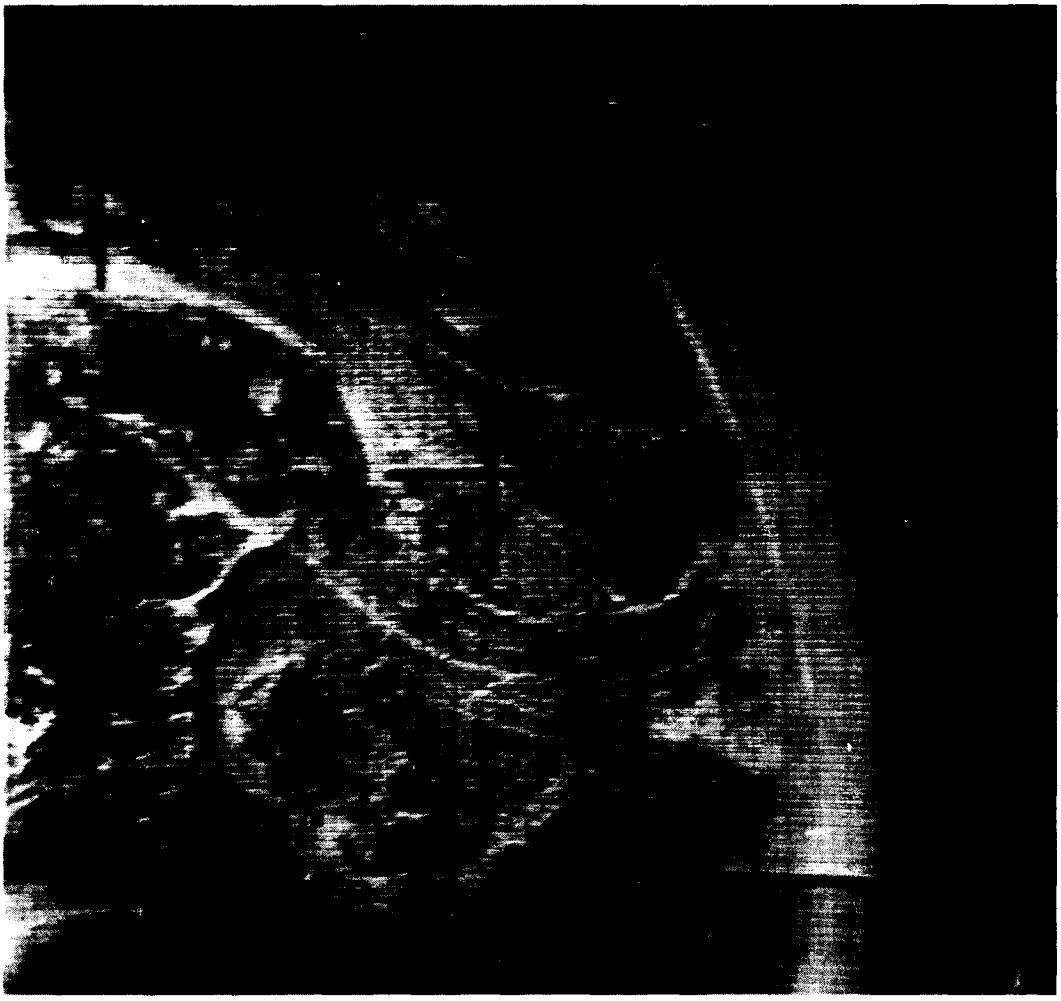

Fig. 11. Tiros-V satellite picture of Gulf of St. Lawrence on February 4, 1963, showing outflow of arctic air over open water causing the development of snow-producing convective bands. Bands measure up to 550 km in length, and are spaced approximately 8 km apart.

The well-known critical Rayleigh number which characterizes the onset of convection in a medium at rest holds also for two dimensional longitudinal rolls. All other convection modes, however, require higher Rayleigh numbers, that is higher vertical density gradients. This is true for three-dimensional cells and for two-dimensional rolls of different orientation, the highest numbers being required for transverse rolls.

In the atmosphere, the observed vertical gradients of wind shear create stabilizing forces which may be of a magnitude comparable to that of the bouyancy forces. Therefore, as solar heating of the ground increases, three-dimensional convection cells may still be entirely suppressed while two-dimensional cells stretching in the wind direction are already highly amplified. Later, three-dimensional convection may also amplify but the growth rates are smaller. Thus longitudinal bands represent the prevailing mode of convection. An approximate theory of this mechanism is given in the next section.

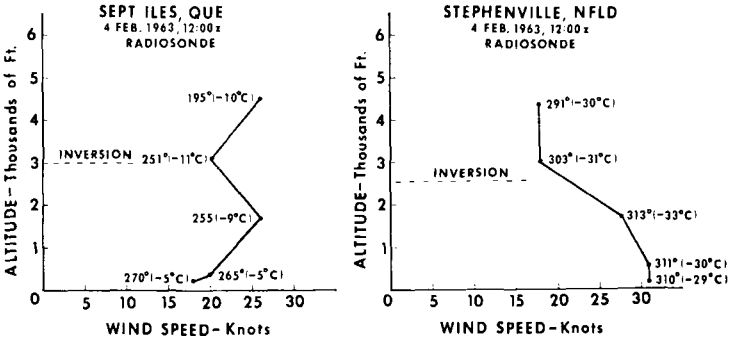

Fig. 12. Rawinsondes taken at Sept Iles, Quebec, and at Stephenville, Newfoundland, (Fig. 11) on February 4, 1963, 12:00 Z. Wind directions and temperatures are marked along curves. Note backing of wind with height.

2. Theory of Convection Bands

The following simplified flow conditions are assumed: an incompressible, viscous and conductive fluid of height H and of infinite horizontal extension flows steadily and under gravity over flat ground in the horizontal x direction. Its speed (but not its direction) varies with height. (See Fig. 15).

The vertical density gradient is constant and positive, setting the stage for convection. It shall be small compared to the density itself. Therefore, their ratio will be neglected everywhere except in its "buoyancy" function, i.e., in connection with gravity. (Boussinesq's approximation; first applied to the problem of cellular convection by Rayleigh, 1916).

It is furthermore assumed that both the kinematic viscosity and the heat diffusivity are invariant throughout the medium and that a linear thermal expansion function holds for the small density changes under consideration.

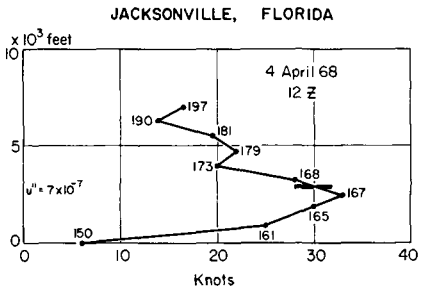

Fig. 14. Rawinsonde taken at Jacksonville, Florida (just south of the lower edge of Fig. 13) on April 4, 1968 at 12:00 Z. Explanations under Fig. 5 apply.

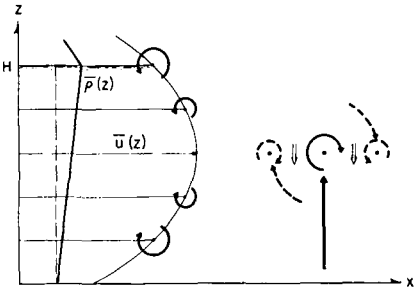

Fig. 15. Schematic presentation of: Basic flow and density profile (left). Relative vorticity of vertically displaced convective element and resulting restoring force (right). See text for further explanation.

The Coriolis force will be neglected as the circulation period of atmospheric convective systems is generally small compared to the inertial period $2\pi/f$ where f = Coriolis acceleration, resulting in large Rossby numbers.

Using small perturbation methods, the properties of the basic flow, to be designated by symbols with a bar ($^-$), shall be functions of height only except the pressure which shall fall off in the flow direction to keep the flow steady against viscosity. Perturbation quantities will be expressed by the same symbols as the basic quantities but without a bar. Prime $(\,)'$ and double prime $(\,)''$ denote first and second derivatives with respect to height.

Using a ground fixed conventional Cartesian coordinate system, x and y, being the horizontal coordinates, u and v the corresponding horizontal velocity components, z the vertical coordinate and w the vertical velocity component, the

Fig. 13. Cloudstreets over Georgia developing near the coastline in a southerly flow on April 4, 1968, as seen from Apollo 6. Maximum length of bands: over 100 km; spacing: 2 to 2.5 km. (Photo NASA.)

profile curvature on the convective modes by the following simplifications:

In analogy to certain boundary layer studies we approximate the height dependent flow velocity $\bar{u}(z)$ by a characteristic mean velocity u of the layer under consideration. Obviously this approximation eliminates any effects of the wind shear $\bar{u}'(z)$.

Likewise, the curvature $\bar{u}''$ of the vertical wind profile shall be expressed by a characteristic mean value $\overline{\bar{u}''}$.

Introducing three-dimensional harmonic perturbations, we leave the door open for an exponential amplification or damping. If l and m are wavenumbers along x and y, and if σ is the exponential time constant, a complex quantity, all perturbations will contain the factor

$$\exp[i(lx+my)+\sigma t]$$

With all basic quantities in (7) now invariant, harmonic variations of w with height are admissable, the phase of which depends on the boundary conditions.

Rayleigh (1916) in his classical theory of cellular convection selected those boundary conditions "which are simplest from the mathematical point of view," namely

$$w - w'' = 0 \quad \text{at } z = 0, H. \tag{9}$$

This corresponds to fixed, "slippery" boundaries. More realistic boundary conditions were later investigated by Jeffreys (1926) and Pellew & Southwell (1940) without affecting the validity of Rayleigh's basic conclusions.

By retaining Rayleigh's boundary conditions, the fundamental difference of convection in a resting and in a moving medium can be demonstrated in the simplets fashion. We therefore apply (9) in this study.

Assuming w proportional to $\sin(nz)$, the above boundary conditions are satisfied by

$$n = r\pi/H \tag{10}$$

where r is an integer. With

$$w'' = -n^2 w$$

the operators used earlier reduce to

$$\left.\begin{aligned} \nabla^2 &= -(l^2+m^2+n^2) \\ \nabla_h^2 &= -(l^2+m^2) \\ f &= \sigma_r + \nu d^2 + is \\ F &= \sigma_r + \varkappa d^2 + is \end{aligned}\right\} \tag{11}$$

Here

$$s = \bar{u}l + \sigma_i = l(\bar{u}-c) \tag{12}$$

σ_r and σ_i are the real and imaginary parts of σ, respectively, and c the phase velocity for waves of wavenumber l. For simplicity, we introduced furthermore the quantity

$$d^2 = (l^2+m^2+n^2) \tag{13}$$

which characterizes the dimensions of a convective cell. Combining (7), (11) and (13)

$$(\sigma_r + \varkappa d^2 + is)\,[(\sigma_r + \nu d^2 + is)\,d^2 + il\bar{u}''] - g\beta(l^2+m^2) = 0 \tag{14}$$

Two cases will be compared: Convection in a resting medium (Rayleigh case) and convection in a flowing medium.

2.1. *Convection in a medium at rest (Rayleigh's case)*

In a resting medium $\bar{u} = \overline{\bar{u}''} = 0$. Considering stationary conditions ($\sigma_i = 0$) (14) reduces to

$$(\sigma_r + \varkappa d^2)\,(\sigma_r + \nu d^2)d^2 - g\beta(l^2+m^2) = 0 \tag{15}$$

which corresponds to equation (37) of Rayleigh (1916) whose results shall be recalled here.

Rayleigh considers the case of "marginal stability" where the maximum amplification

$$\sigma_{\max} = 0$$

In this case optimum cell dimensions are given by

$$\zeta = n^2/d^2 = 2/3 \tag{17}$$

resulting in the well-known "critical Rayleigh number",

$$R_0 = g\beta/\varkappa\nu n^4 = [\zeta^2(1-\zeta)]^{-1} = 27/4 = 6{,}75 \tag{18}$$

The mode of greatest instability is that for which n is smallest,

$$\text{i.e. } r = 1, \quad \text{see (10).}$$

With

$$n = \pi/H \tag{19}$$

the critical Rayleigh number as expressed by

$$R_0^* = g\beta H^4/k\nu = 27\pi^4/4 \approx 658 \tag{20}$$

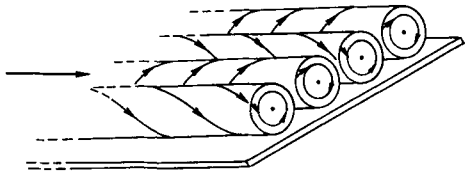

Fig. 16. Longitudinal cells with helical motions (also called "rolls," "streets," "lines", "bands", "strips").

The corresponding values for more realistic boundary conditions (both boundaries fixed, or one free/one fixed, see Jeffreys, 1926; Pellew & Southwell, 1940) range from 1 100 to 1 700.

It has been noticed by Rayleigh that only the value of the sum (l^2+m^2) is determined by the stability criterion, but not l^2 and m^2 separately.

For example, two-dimensional cells, i.e., convection bands (also called "rolls," "lines", "strips", "streets") would be equally amplified as three-dimensional cells ("symmetrical cells"), Fig. 16 and 17, but their spacing would be different. Bands would have a wavelength

$$\lambda_b = 2\sqrt{2}\,H \qquad (21$$

symmetrical cells a wavelength

$$\lambda_s = 4\,H \qquad (22)$$

as follows from (13), (17), and (19).

Rayleigh states this "uncertainty principle" as follows: "I do not see that any plausible hypothesis as to the origin of the initial disturbances leads us to expect one particular ratio of sides in preference to another."

This situation changes drastically if convection takes place in a flowing medium.

2.2 *Convection in a flowing medium*

To solve the more general equation (14) where $\bar{u}, \overline{u''} \neq 0$ we neglect, in a first approximation, the difference between the diffusivities for momentum and heat, and assume the Prandtl number

$$P_r = \nu/k = 1 \qquad (23)$$

Since the parameters f and F are now identical, one may introduce the quantity

$$\gamma = fd^2 = Fd^2 = (\sigma_r + \nu^* d^2 + is)d^2 \qquad (24)$$

Here

$$\nu^* = (k\nu)^{\frac{1}{2}} \qquad (25)$$

It should be remembered that both heat conductivity and viscosity have been taken into account here, but that they are assumed to be numerically equal.

Introducing (24) into (14) the following quadratic equation results

$$\gamma^2 + il\,\overline{u''}\gamma - g\beta(l^2+m^2)d^2 = 0 \qquad (26)$$

The amplification contant is now given by

$$\sigma_r = \mp\left[g\beta(l^2+m^2)/d^2 - (l\overline{u''}/2d^2)^2\right]^{\frac{1}{2}} - \nu^* d^2 \qquad (27)$$

which is the real part of the solution of (26). This relation between amplification and cell size in non-uniform flow was already cited in Part I and will now be discussed.

The choice of sign in front of the bracket indicates the possibility of a positive growth rate.

The first term in the bracket containing gravity and density gradient represents the buoyancy. Its magnitude depends on the cell dimensions such that, with decreasing horizontal cell size (increasing l and m) the term tends towards a finite maximum value, namely $g\beta$ while it tends toward zero with increasing cell size.

The second expression in the bracket is the vorticity term. Regardless of the sign of the shear gradient, $\overline{u''}$, this term always subtracts from the buoyancy. If larger than the buoyancy term, the vorticity term is responsible for waves of the type mentioned earlier. Due to the presence of vorticity, the real part of the bracket may vanish at finite values of l.

The last term (27), the viscosity/conductivity term, is always negative and tends to suppress or dampen buoyant motions. For decreasing cell size (increasing l and m) it tends toward $-\infty$ while, for increasing cell size, it approaches the finite negative value, $-\nu^* n^2$.

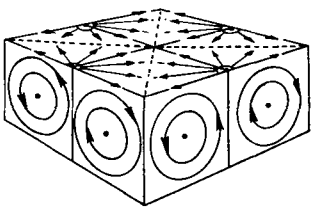

Fig. 17. Symmetric cells.

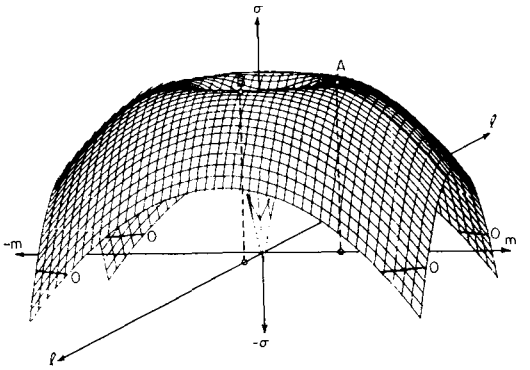

Fig. 18. Three-dimensional computer presentation of growth rate σ as a function of horizontal wave numbers l and m (equation 27) for a medium of rest. The maximum growth rate is given by a circular ridge (A, B) defined by a certain value of $(l^2 + m^2)$. Rayleigh's case.

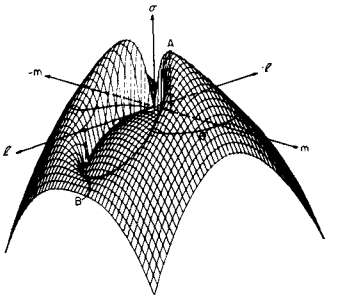

Fig. 19. Same as Fig. 18, but a for flowing medium (equation 27). The maximum growth rate holds only for $l = 0$ (point A), i.e. for longitudinal cells (l is the wave number along the flow direction). For $m = 0$, i.e. for transverse cells, the growth rate is negative (Point B).

This brings us to the general behavior of the growth rate σ_r in (27) as a function of the horizontal wave numbers l and m.

General behavior of growth rate as a function of wave numbers. The behavior of this function can best be visualized by a three-dimensional computer presentation of equation (27). Fig. 18 shows the case of a medium at rest, Fig. 19 that of a flowing medium. In both cases, the mushroom like body has the following characteristics:

In the center, that is at $m = l = 0$, σ is negative. (From now on, σ_r will be replaced by σ with the understanding that we are dealing with a real quantity.) At this point the horizontal wavelengths tend towards infinity and correspond to one unlimited symmetric convective cell. Due to vanishing buoyancy and the presence of viscosity/conductivity the motion dies out. On the outside, as l and m grow without limit (the cells getting narrower) σ tends toward minus infinity. Here the motion again dies out, due to the action of conductivity and viscosity and rapidly increasing gradients of temperature and velocity among cells.

Between these two extremes, there is a range of cell dimensions where σ reaches a maximum which may be positive depending on the magnitude of β in the buoyancy term.

If the medium is *at rest* the maximum of σ is characterized by a circular ridge of constant elevation (Fig. 18). The radial nature of this ridge indicates that maximum amplification is the same over the m-axis (point A) as over the l-axis (point B) and applies to any combination of l and m resulting in a certain critical value of $(l^2 + m^2)$. This illustrates that there is no preference for a definite ratio of the cell sides (Rayleigh's "uncertainty principle", see p. 417 above).

In a *flowing* medium (Fig. 19) the ridge of maximum amplification is deformed by the vorticity term. Slopes develop toward the l axis such that saddle points (B) form there while position and elevation of the maxima over the m axis (A) remain unchanged.

The emerging cell form is now uniquely determined by point A and the condition $l = 0$, which corresponds to two-dimensional convection bands stretching without limit in the direction of flow (longitudinal bands). In contrast the saddle point B signifies that convection bands stretching normal to the flow

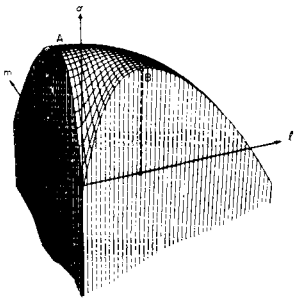

Fig. 20. Quadrant with positive wave numbers l and m of Fig. 18.

direction (transverse bands) are least amplified or, as in Fig. 19, damped. It will be noticed that the center area in Fig. 19 has the appearance of a "cushion", the center point being a saddle, while in Fig. 18 no such "cushion" exists and the center point represents an absolute minimum. This is due to the fact that the bracket in (27) reaches zero at finite values of l, if the vorticity term is $\neq 0$, in this way exposing the bell-shaped viscosity term (Fig. 19). In contrast the bracket in (27) reaches zero at the origin, if the vorticity term is zero, in this way exposing the funnel-shaped buoyancy term (Fig. 18) with a minimum at the center.

Since only positive wave numbers are of interest here, the positive quadrants of Fig. 18 and 19 are reproduced in Figs 20 and 21. A plane view of Fig. 21 gives the contours of the growth rate σ in the l/m plane for the case of the flowing medium (Fig. 22). As can be seen σ varies, in the selected case, from $+2.3 \times 10^{-3}$ $\sec^{-1}$ for longitudinal bands to about -1.7×10^{-3} $\sec^{-1}$ for transverse bands, while symmetric cells ($l = m$) are nearly neutral. The example chosen will be discussed later.

The behavior of the growth rate σ illustrated in these figures will now be derived more rigorously from equation (27).

Convection pattern in a flowing medium. Introducing the quantity

$$\varphi = [g\beta(1-\zeta) - (l\bar{u}''/2d^2)^2]^{\frac{1}{2}} \tag{28}$$

where ζ is defined by (17), equation (27) may be rewritten as

$$\sigma = \mp\varphi - \nu^* d^2 \tag{29}$$

Cell dimensions l and m yielding maximum growth rate σ, as determined by

$$\partial\sigma/\partial l = \partial\sigma/\partial m = 0$$

are given by

$$\{[(\psi - \bar{u}''^2/4)/\varphi d^4] - 2\nu^*\} l = 0 \tag{30}$$

and

$$[(\psi/\varphi d^4) - 2\nu^*] m = 0 \tag{31}$$

Here

$$\psi = g\beta n^2 + l^2\bar{u}''^2/2\,d^2 \tag{32}$$

The following alternatives result:

$$l = m = 0 \tag{33}$$

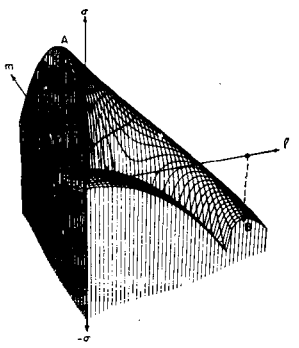

Fig. 21. Quadrant with positive wave numbers l and m of Fig. 19.

$$l = 0;\ (\psi/\varphi d^4) = 2\nu^* \tag{34}$$

$$m = 0;\ (\psi - \bar{u}''^2/4)/\varphi d^4 = 2\nu^* \tag{35}$$

The remaining alternative may be interpreteted as the case treated by Rayleigh with $\bar{u}'' = 0$, since both (30) and (31) are then satisfied by the single condition

$$\psi = 2\varphi d^4\,\nu^*$$

(Rayleigh's criterion) and l and m remain indeterminate.

Obviously, the first alternative, (33), represents the negative center cf Figs. 18 and 19,

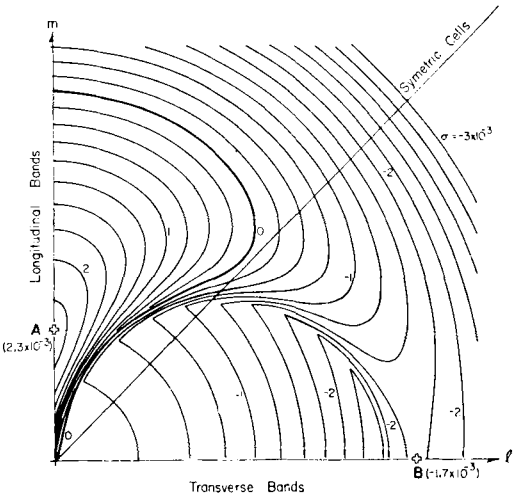

Fig. 22. Plane view of Fig. 21. showing the contours of the growth rate σ as a function of wave numbers l and m. Longitudinal bands are highly amplified (A), symmetrical cells are nearly neutral, transverse bands are highly damped (B).

corresponding to a convection cell of infinite horizontal extension.

Here

$$\sigma = -\nu^* d^2$$

and the motion is damped.

Case (34) represents the peak A of σ along the m axis and corresponds to longitudinal bands, while case (35) corresponds to the saddle point B along the l axis and represents bands across the flow direction ("transverse bands"), see Figs. 19, 21 and 22.

Case 1. Bands along flow direction (longitudinal bands). Taking alternative (34) first and introducing it into (29), under the condition of marginal stability given by (16), we obtain

$$\psi = 2\varphi^2 d^2$$

Substituting (28) and (32), with $l = 0$ and $m \neq 0$, the cell dimensions are determined by the relation

$$\zeta \equiv n^2/d^2 = 2/3 \tag{36}$$

This is identical with Rayleigh's case, see (17). Introduction of (36) into (29), for $\sigma = 0$ yields as critical Rayleigh number R_c the same value as was derived for a medium at rest, see (18):

$$R_c = R_0 \tag{37}$$

Now, however, Rayleigh's undeterminedness regarding the ratio of cell sides is removed. There is no question anymore whether (21) or (22) applies. With $l = 0$, the convection cells are bands along the flow direction and their approximate spacing as given by (21) is

$$\lambda_b = 2.8\, H \tag{38}$$

under the assumed boundary conditions. Fig. 16 illustrates this case.

Case 2: Bands across the flow direction (transverse bands). We now turn to the other alternative, (35) and introduce it into (29), again implying "marginal stability." We obtain

$$\psi - \overline{\tilde{u}''^2}/4 = 2\varphi^2 d^2$$

Substituting (28) and (32), where $m = 0$ and $l \neq 0$

$$\zeta[1 + (1/4 - \zeta/3)\varepsilon] = 2/3 \tag{39}$$

where

$$\varepsilon = \overline{\tilde{u}''^2}/g\beta n^2 \tag{40}$$

ε relates inertia to buoyancy forces and may be considered as a *Froude number* (or the reciprocal of a modified Richardson number). It is the appearance of inertia forces expressed by ε which is responsible for the changes in the cellular pattern from a medium at rest.

Comparing (39) and (36) it is seen that the cell dimensions are modified by ε such that for

$$\varepsilon > 0, \quad \zeta < 2/3 \tag{41}$$

and the spacing of transverse bands is reduced in comparison with longitudinal bands.

Introducing (39) into (29) for $\sigma = 0$ (marginal stability) the critical Rayleigh number R_0 defined in (18) is modified by ε to

$$R_c = [\zeta^2(1-\zeta)\,(1 - \zeta\varepsilon/4)]^{-1} \tag{42}$$

For small ε, this reduces, in view of (39), to

$$R_c \approx R_0(1 + \varepsilon/6) \tag{43}$$

and for large ε to

$$R_c \approx R_0(\varepsilon/4)^2 \tag{44}$$

It is clear then that in this case the critical Rayleigh number for transverse bands grows approximately with the 4th power of the profile curvature $\overline{\tilde{u}''}$, strongly penalizing the transverse mode against the longitudinal mode. The corresponding equation for symmetrical (square) cells is:

$$R_c = [\zeta^2(1-\zeta)\,(1 - \zeta\varepsilon/8)]^{-1} \tag{45}$$

Functions (42) and (45) are plotted in Fig. 23 which shows the ratio of the critical Rayleigh number R_c to the unmodified Rayleigh number R_0, defined in (18), as a function of the Froude number ε for longitudinal, transverse and symmetrical cells. It can be seen that a given Rayleigh number may well be supercritical for the longitudinal mode, but subcritical for the transverse or symmetrical mode. In this way longitudinal bands are first amplified and emerge as the prevailing convection pattern in a flowing medium.

III. Discussion

The formation of longitudinal convection bands as derived in the previous section is closely related to the well-known Goertler instability over curved boundaries (Goertler, 1940) and to Taylor's (1923) experiments with rotating cylinders. In both cases the formation of longitudinal rolls is controlled by a dimensionless number of the form

$G = Re\sqrt{l/r}$ (Goertler number)

where Re = Reynolds number, l = layer depth and r = radius of curvature. Jeffreys (1928) and Goertler (1959) have already recognized the equivalence of inertia and buoyancy forces in creating this type of instability.

The Goertler number can be understood to be the square root of a product of the regular Reynolds number and a modified Reynolds number which relates centrifugal forces $\bar{u}^2/r$ to viscosity forces $\nu\bar{u}/l^2$. Replacing the centrifugal force by the buoyancy force $g\beta H$ and substituting H for l one obtains the Grasshof number

$$Gr = g\beta H^4/\nu^2$$

which, for a Prandtl number of unity, see (23), is identical with the Rayleigh number defined in (20).

Even quantitatively there is rough agreement. With the critical Goertler and Taylor numbers, G_0, ranging from about 10 to 40 (Schlichting, 1960)—provided they are applied to the appropriate layer depth—we find approximately

$$R_0 \approx G_0^2$$

As has been pointed out earlier, linear wind shear has been shown to exert similar "streeting" effects on convection as the shear gradient. (Kuo, 1963; Deardorff, 1965; Gallagher & Mercer, 1965; Asai, 1970). At first glance it appeared that the shear term had dropped out by the operation leading to equation (6). However, a height-dependent basic flow $\bar{u}(z)$ was still contained in (7). As mentioned before, it was the simplification of introducing a characteristic mean velocity $\bar{u}$ which eliminated the effect of shear (but facilitated the treatment of curvature). Obviously the vorticity gradient $\overline{\bar{u}''}$ contains shear by definition, but in addition it can be connected with small or large *average* shear (see for example Fig. 12, as compared with Fig. 14). A more complete theory covering the effects of both shear and shear gradient should establish their relation more clearly. The physical mechanisms involved in the two cases appear to be quite different.

Our results may be compared with those of Gage & Reid (1968) who investigated the case of thermally stratified Poisseuille flow. Their stability boundaries, presented as a function of Reynolds and Rayleigh numbers, depend on the orientation of the two-dimensional disturbances (or their three-dimensional equivalents). The shapes of these boundaries are different from ours, due to the fact that, in addition to convective cells, the formation of two-dimensional Tollmien-Schlichting waves was included. Their analysis shows that for such waves the most unstable mode is the transverse disturbance—independent of the Rayleigh number—while for thermal convection the most unstable mode is the longitudinal disturbance—independent of the Reynolds number. Thus, for sufficiently high Reynolds numbers, Tollmien-Schlichting waves could form at Rayleigh numbers which are higher than the critical Rayleigh number of longitudinal cells, but lower than the critical Rayleigh number of transverse cells. These waves would be superimposed on longitudinal convection rolls. Such patterns are occasionally observed under cloudstreet conditions. (Malkus & Riehl, 1964). The Apollo 9 photo, Fig. 24, taken by the astronauts over the BOMEX area suggests a formation of this type. Generalisation to more arbitrary wind profiles and a corresponding growth rate analysis are now needed.

IV. Application to the Atmosphere

Application of the theory of Section II to the earth's atmosphere requires care. Especially difficult are quantitative estimates.

As in other incompressible theories the positive density gradient needs to be replaced by the negative gradient of potential temperature θ so that

$$\beta = -\bar{\theta}'/\bar{\theta} \qquad (46)$$

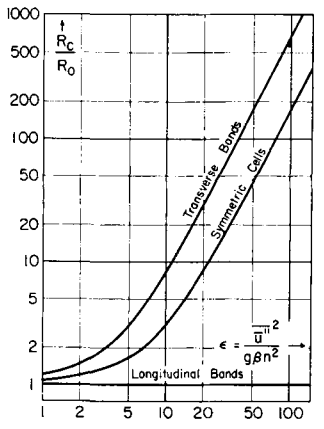

Fig. 23. Ratio of critical Rayleigh number R_c, as defined by equations (42) and (45), to unmodified Rayleigh number R_0, as defined by equation (18), as a function of Froude number ε. Depending on the profile curvature $\overline{u}''$, contained in ε, transverse bands and symmetric cells require higher critical Rayleigh numbers than longitudinal bands.

Molecular viscosity and heat conductivity have to be replaced by eddy diffusivities which in turn are a function of convective turbulence. The assumption (23) of a Prandtl number of unity may, under these conditions, hold better than in the molecular case, especially in near neutral air (Lumley & Panofsky, 1964).

Regarding the simplified boundary conditions used in the above theory, they are not directly applicable to atmospheric convection over oceans and land where a quasi-fixed lower and a quasi-free upper boundary exists. The latter usually consists of a temperature inversion or stably stratified layer. This will change the value of the critical Rayleigh number, but not invalidate the physical picture, as Jeffreys (1928) and Southwell & Pellew (1940), following Rayleigh's (1916) simplified theory, have shown. Rayleigh's boundary conditions have been used here for reasons explained earlier. Refinement of the theory for more realistic boundary conditions is required.

A complication is introduced by atmospheric condensation which, unfortunately, is the only simple way to make atmospheric convection modes visible. Glider experience, however, shows that dry "updraft streets" form under similar conditions as cloudstreets, allowing the glider pilot to fly straight under clear skies, rather than to circle in thermals. This is confirmed by Konrad's (1968) radar observations of thermal streets in clear air.

The effect of condensation is two-fold: It introduces a buoyancy source at an elevated level and it extends convection upwards into a layer which is unstably stratified inside clouds and stably stratified outside. This situation also affects the eddy diffusivity which will tend to have higher horizontal than vertical components. As Kuo (1965) has shown, the effect of a conditionally unstable atmosphere in stable surroundings is to increase the area of descending currents in comparison to that of ascending currents. The non-isotropy of eddy diffusivities also tends to enlarge the spacing between upcurrents. The effect is minimized if the clouds are shallow.

To test the significance of the velocity profiles observed in the atmosphere, some quantitative estimates can be made with respect to the Rayleigh number

$$R = g\beta/\nu^{*2}n^4, \tag{47}$$

see (18) and (25), and the Froude number

$$\varepsilon = \overline{u}''^2/g\beta n^2 \tag{48}$$

see (40). Obviously R will be smallest and ε largest when convection begins to develop, since $g\beta$ will be quite small. As a consequence, the influence of the wind profile on the critical Rayleigh number and on the mode of convection will be maximized, as Fig. 23 shows.

Longitudinal rolls will therefore develop in the early stages of convective activities. Later on, also other modes may be excited but to a lesser degree than the longitudinal modes.

Superadiabatic temperature gradients in the dry atmosphere are notoriously difficult to measure—except in the layer immediately adjacent to the ground—because the deviations from the dry-adiabate are within the error of the temperature elements of standard radio sondes (about 0.5°C). We are therefore justified to assume that the vertical potential temperature gradient θ' is smaller than 0.5°/km. Keeping in mind that this should be an average value throughout the convective layer, including areas of ascending and descending motion, θ' is probably quite small. The quantity $g\beta$ should then be of the order of 10^{-5} sec^{-2} or smaller. Great difficulty is also encountered in arriving at valid estimates of eddy diffusivities for momentum and heat, especially since the concept of eddy viscosity in the planetary

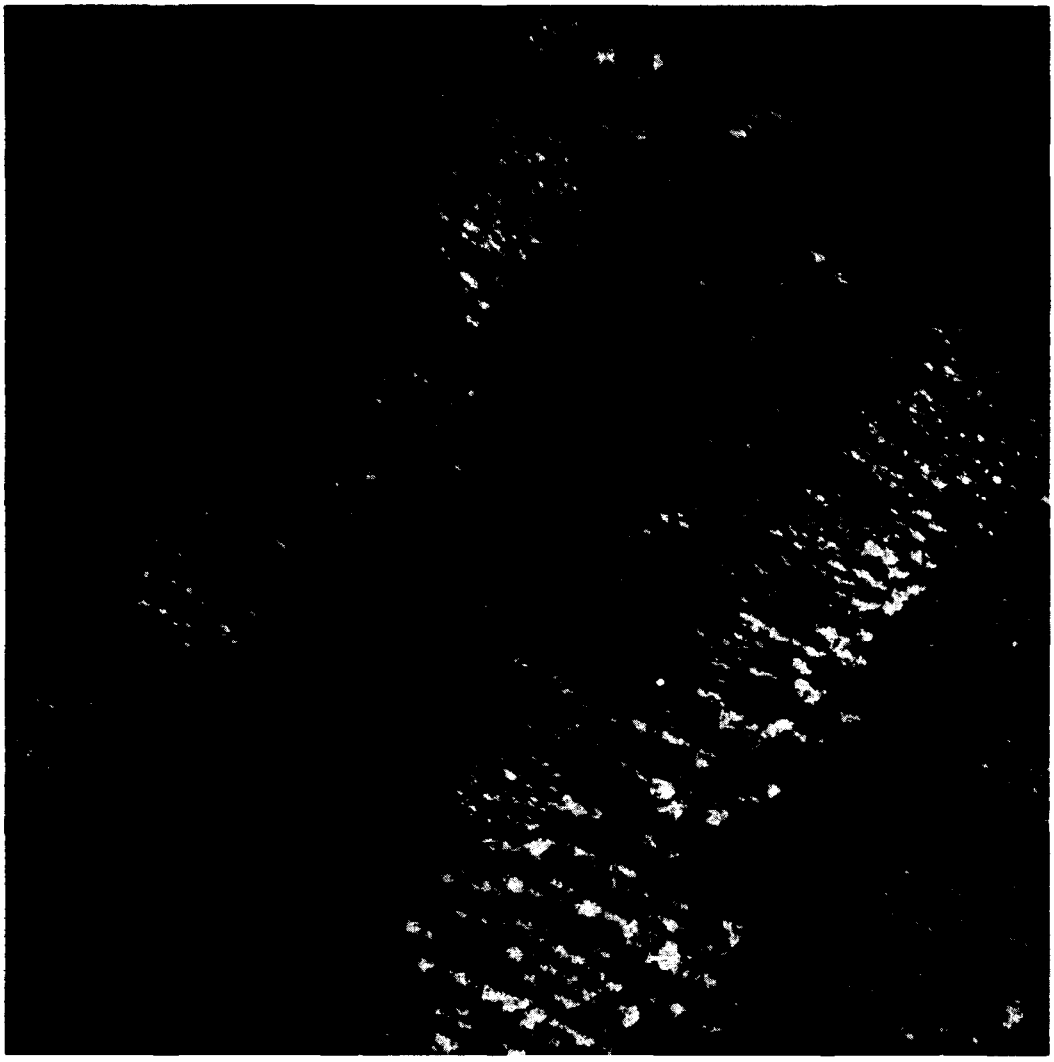

Fig. 24. Cloud development near BOMEX area as photographed by the Apollo-9 astronauts (Photo NASA).

boundary layer needs improvement. Under convective conditions we may assume that

$$10^4 < \nu^* < 10^6 \text{ cm}^2 \text{ sec}^{-1}$$

A value of 10^5 cm^2 sec^{-1} will be adapted here. From the observations described in Section I, we may assume a layer height of the order of 1 km.

With these values the Rayleigh number defined in (47) is of the order of 10^3. Since the critical Rayleigh number $R_0 = 6.75$, see (18), the quantity $R/R_0 \approx 150$, see Fig. 23.

The observed vorticity gradient $\overline{\tilde{u}''}$ ranges from 10^{-7} to 10^{-6} cm^{-1} sec^{-1}. The computer presentations, Figs. 19, 21, and 22, use the upper value. In this case $\varepsilon \approx 100$ and the critical Rayleigh number R_c for symmetric cells is a little over 150 (see Figs. 22, 23), i.e. $R/R_c \approx 1$. Symmetric convection therefore has neutral stability. In contrast transverse cells have a critical Rayleigh number of 600 resulting in $R/R_c = 0.25$ and the growth rate $\sigma = -1.7 \times 10^{-3}$ sec^{-1}. Therefore transverse rolls are highly damped, their amplitude decaying with a half-life of about 7 min. Since the Froude number, ε,

is proportional to Re^2/R it is possible that Tollmien–Schlichting waves develop for the transverse mode of supercritical Reynolds numbers (see Section III). For longitudinal rolls in turn $R_c = R_0$ and the existing Rayleigh number R is highly supercritical for this mode. ($R/R_c = 150$). Thus, convection bands have a growth rate $\sigma = +2.3 \times 10^{-3}$ and may double their amplitude in a little over 5 min. The actually observed values of $\overline{u''}$ (see Section I) lie between 2 and 7×10^{-7} corresponding to a range of ε from 4 to 50 with somewhat less dramatic contrasts between the different convection modes.

It should be kept in mind that, due to the high powers involved in the dimensionless numbers, all values are highly sensitive to the uncertainties in the assumed magnitude of the quantities β, ν, n and $\overline{u''}$. Therefore, the examples chosen should be considered as qualitative illustrations of a largely unknown atmospheric process.

The observed "width/height" ratio of cloud streets (2 to 4) corresponds satisfactorily to the expected theoretical value of 2.8, see (21) for steady convection and to laboratory experiments with curved velocity profiles (Avsec, 1939). In this connection a remark on the assumed exponential growth rate, see discussion between equations (8) and (9), is in order. Both atmospheric and laboratory observations suggest that in reality a new steady state is approached when the convective perturbation velocities have reached sufficiently high values to accomplish the required heat transport. The theoretical width/height ratio for the case $\sigma = 0$ may then be expected again.

It should be mentioned here that the above theory may also apply to the wind streaks often observed on lake and ocean surfaces (Roll, 1965). One may speculate that the wind stress on the water surface will result in a curved velocity profile in the upper layers of the water while evaporative cooling of the water surface will favor unstable stratification. If turbulent mixing takes place—which can be expected under high wind conditions and may actually define a threshold value for the wind speed—a deep mixing layer will form and the assumption of a Prandtl number of unity will also be justified. The spacing of the streaks which represent helical circulations (Langmuir, 1938) will then depend on the depth of the mixed layer and should be a multiple of it.

Acknowledgements

The writer expresses his gratitude to Professor R. Pierce for his valuable suggestions and to Dr. R. Slutz for his kind cooperation in the generation of three-dimensional computer presentations.

REFERENCES

Alaka, Queney, et al. 1960. *The air flow over mountains.* WMO Tech. Note No. 34, Geneva.

Anderson, R. K., Ferguson E. W. & V. J. Oliver. 1966. *The use of satellite pictures in weather analysis and forecasting.* WMO Tech. Note. No. 75, Geneva. WMO No. 190, 96 pp.

Anderson, R. K. et al. 1969. *Application of meteorological satellite data in analysis and forecasting.* ESSA Technical Report. NESC 51.

Angell, J. K., Pack, D. H. & Dickson, C. R. 1968. A Lagrangian study of helical circulations in the planetary boundary layer. *J. Atmos. Sci. 25*, 707–717.

Asai, T. 1970. Three-dimensional features of thermal convection in a plane Couette flow. *J. Met. Soc. Japan 48*, 18–29.

Avsec, D. 1939. *Tourbillons thermoconvectifs dans l'air.* Thèses de la faculté des Sciences de l'Université de Paris. Serie A., No. 1910, pp. 214.

Barcilon, V. 1965. Stability of non-divergent Ekman layers. *Tellus 17*, 53–68.

Brown, R. A. 1970. A secondary flow model for the planetary boundary layer. *J. Atmos. Sci. 27*, 742–757.

Benard, H. 1900. Les tourbillons cellulaires dans une nappe liquide. *Rev. gen. sci. pur. appl. II*, 1261–1271; 1309–1328.

Benard, H. 1927. Sur les tourbillons en bandes et la théorie de Rayleigh. *C. R. Acad. Sci. Paris 185*, 1257–1259.

Brunt, D. 1951. Experimental cloud formation. *Compendium of Meteorology*, p. 1255–1262.

Chandra, K. 1938. Instability of fluids heated from below. *Proc. Roy. Soc. A 164*, 231–242.

Deardorff, J. W. 1965. Gravitational instability between horizontal plates with shear. *Phys. Fluids 8*, 1027–1030.

Faller, A. J. 1963. An experimental study of the instability of the laminar Ekman boundary layer. *J. Fluid. Mech. 15*, 560–576.

Faller, A. J. 1965. Large eddies in the atmospheric boundary layer and their possible role in the formation of cloud rows. *J. Atmos. Sci. 22*, 176–184.

Faller, A. J. & Kaylor, R. E. 1966. A numerical study of the instability of the laminar Ekman boundary layer. *J. Atmos. Sci. 23*, 466–480.

Gaby, D. C. 1967. Cumulus cloud lines vs. surface wind in equatorial latitudes. *Mon. Weath. Rev. Wash. 85*, 203–208.

Gage, K. S. & Reid, W. J. 1968. The stability of thermally stratified plane Poiseuille flow. *J. Fluid Mech. 33*, 21–32.

Gallagher, A. P. & Mercer, A. Mcd. 1965. On the behaviour of small disturbances in plane Couette flow with a temperature gradient. *Proc. Roy. Soc. A 286*, 117–128.

Gifford, F. A. 1953. A study of low-level air trajectories at Oak Ridge, Tenn., *Mon. Weath. Rev. Wash. 81*, 179–192.

Goertler, H. 1940. Über eine dreidimensionale Instabilität laminarer Grenzschichtströmungen an konkaven Wänden. *Nachr. Ges. Wiss. Goettingen, Math.*-Phys. Klasse, Neue Folge *1*, 2.

Goertler, H. 1959. Über eine Analogie zwischen den Instabilitäten laminarer Grenzschichtströmungen an konkaven Wänden und an erwärmten Wänden. *Ing. Arch. 28*, 71–78.

Graham, A. 1933. Shear patterns in an unstable layer of air. *Phil. Trans. Roy. Soc. London 232*, 285–290.

Hanna, S. 1969. The formation of longitudinal sand dunes by large helical eddies in the atmosphere. *J. Applied Met. 8*, 874–883.

Jeffreys, H. 1928. Some cases of instability in fluid motion. *Proc. Roy. Soc. A 118*, 195–208.

Konrad, T. G 1968. The alignment of clear air convective cells. *Proc. Intl. Conf. Cloud Physics*, Toronto, Canada, 539–543.

Kuettner, J. P. 1949. Der Segelflug in Aufwindstrassen. *Schweiz. Aerorev. 24*, 480–482.

Kuettner, J. P. 1959. The band structure of the atmosphere. *Tellus 11*, 267–294.

Kuettner, J. P. & Soules, S. D. 1966. Organized convection as seen from space. *Bull. Amer. Meteor. Soc. 47*, 364–370.

Kuettner, J. P. 1967. Cloudstreets, theory and observations. *Aero Revue 42*, 52–56, 109–112.

Kuo, H. 1963. Perturbations of plane Couette flow in stratified fluid and origin of cloud streets. *Physics of Fluids 6*, 195–211.

Kuo, H. 1965. Further studies of the properties of cellular convection in a conditionally unstable atmosphere. *Tellus 17*, 413–433.

Langmuir, I. 1938. Surface motion of water induced by wind. *Science 87*, 119–123.

Lilly, D. K. 1966. On the stability of Ekman boundary flow. *J. Atmos. Sci., 23*, 481–494.

Lin, C. 1955. *The theory of hydrodynamic stability.* Cambridge University Press. 155 pp.

Lumley, J. & Panofsky, H. 1964. *The structure of atmospheric turbulence.* Wiley, New York. 231 pp.

Mal, S. 1930. Forms of stratified clouds. *Beitr. Phys. frei. Atmos. 17*, 40–70.

Malkus, J. S. & Riehl, H. 1964. *Cloud structure and distributions over the tropical Pacific Ocean.* University of California Press, Berkeley and Los Angles. 229 pp.

Pellew, A. & Southwell, R. 1950. On maintained convective motion in a fluid heated from below. *Proc. Roy. Soc. A176*, 312–343.

Plank, V. G. 1966. Wind conditions in situations of patternform and non-patternform cumulus convection. *Tellus 18*. 1–12.

Rayleigh, Lord. 1916. On convection currents in a horizontal layer of fluid, when the higher temperature is on the underside. *Phil. Mag.* (Series 6) *32*, 529–546.

Roll, H. 1965. *Physics of the Marine Atmosphere.* Academic Press, New York. 426 pp.

Schlichting, H. 1960. *Boundary layer theory.* McGraw-Hill, New York. 630 pp.

Schuetz, J. & Fritz, S. 1961. Cloud streets over the Caribbean Sea. *Mon. Weath. Rev. 89*, 375–382.

Taylor, G. I. 1923. Stability of a viscous liquid contained between two rotating cylinders. *Phil. Trans. A 223*, 289–343.

Terada, T. 1928. Some experiments on periodic columnar forms of vortices caused by convection. *Report Aeron. Res. Inst., Tokyo, Imp. Univ. 3*, 1–46.

Woodcook, A. 1941. Soaring over the open sea. *Sci. Mon. 55*, 226–232.

ОБЛАЧНЫЕ ПОЛОСЫ В ЗЕМНОЙ АТМОСФЕРЕ. НАБЛЮДЕНИЯ И ТЕОРИЯ

Теперь хорошо известно, что параллельные полосы облаков широко распространены в земной атмосфере. Наблюдения с управляемых и автоматических космических кораблей и с высотных самолетов вместе с зондированием с судов и наземных станций пролили свет на их происхождение. Эти и специальные исследования тропических дорожек облаков во время проекта БОМЭКС дают следующие типичные характеристики конвективных облачных дорожек: длина от 20 до 500 *км*, разделение от 2 до 8 *км*, высота слоя от 0,8 до 2 *км*, отношение ширины к высоте от 2 до 4, структура ветра — малое изменение направления с высотой, вертикальный градиент сдвига ветра (кривизна профиля) от 10^{-7} до 10^{-6} $см^{-1}$ $сек^{-1}$, вытянутость — вдоль среднего ветра в конвективном слое.

С теоретической стороны известно, что линейный сдвиг ветра по высоте благоприятствует образованию конвективных дорожек. В настоящей работе исследуется эффект наблюдаемой кривизны профиля в пренебрежении эффектами линейного по высоте сдвига ветра. Показано, что кривизна сама по себе вызывает вытягивание конвективных ячеек в направлении среднего потока. Инерциальные силы, возникающие в вихревом поле, противодействуют силам плавучести. Их отношение, выраженное как модифицированное число Фруда, определяет величину критического числа Рэлея, ответственного за возникновение конвекции. В движущейся среде это число увеличивается, часто на несколько порядков, по сравнению с его значением в покоящейся среде, для

всех конвективных мод, за исключением продольной моды. Для иллюстрации этих положений приведены результаты некоторых трехмерных численных расчетов.

Предпринята попытка количественного использования результатов упрощенной теории к реальным атмосферным условиям. Получено, что для быстрых течений, подогреваемых снизу, продольные возмущения могут удвоить свою амплитуду за время порядка 10 минут, в то время как поперечные возмущения затухают с такой же скоростью, причем симметричные ячейки близки к нейтральной устойчивости.

Обсуждаются также связи этой концепции с другими гипотезами и с возмущениями Гертлера–Тэйлора. Наконец, приводятся спекуляции, что формирование ветровых полос на поверхности воды может быть связано с аналогичным механизмом.